AIAA JOURNAL
Vol. 44, No. 11, November 2006

Multiple Delamination Detection of Composite Beam Using Magnetostrictive Patch

Ping Tan* and Liyong Tong†
University of Sydney, Sydney, New South Wales 2006, Australia

DOI: 10.2514/1.23050

This paper deals with detection of multiple through-the-width delaminations for a laminated beam using smart magnetostrictive material patches. A dynamic analytical model is developed using the classical beam theory and the assumption of constant peel and shear strains through bond line thickness. A magnetostrictive patch is perfectly bonded on the top surface of a host laminated beam. One of the magnetostrictive patch segments is employed as an actuator to excite the beam system, whereas the rest are employed as sensors to measure the required magnetic flux density passing through each magnetostrictive patch segment. A typical multiple delamination pattern, namely the original-pattern, is considered in this investigation. By monitoring the variation trend of magnetic flux density distributions along beam length, multiple delaminations within a laminated beam system can be clearly identified. A comparison of the first three frequencies between the present analytical and finite element analysis models shows that there is a good agreement between these two models.

I. Introduction

DELAMINATION may result from foreign object impact, poor manufacturing process, stress concentrations at the free edge, local or global buckling of laminated composites, and fatigue from environmental cycling. Low velocity foreign object impact is considered as one of the major causes for delamination. In general, delaminations occur subsurface and are usually barely visible. The presence of delamination can significantly reduce the compression-after-impact strength of laminated composites, and thus can severely reduce their load-carrying capability or compromise structural reliability and safety. To improve the safety and serviceability of laminated structures, it is important to develop reliable and effective nondestructive techniques and methods for detecting delaminations.

Over the past decade, there has been a considerable volume of work for development of methods and techniques for delamination detection, such as the lamb wave method [1–3], vibration based method [4–6], electric resistance change method [7–10], delamination detection methods using fiber bragg grating sensors [11,12], and those using piezoelectric sensors with distributed electrode strips [13–15]. However, all of them deal with an idealized case of single delamination, and there is only limited attention to multiple delamination detection for laminated structures.

Recently, investigation of multiple delaminations for laminated composites has drawn more and more attention. For example, Parhi et al. [16–18] developed a simple multiple delamination model for dynamic analysis of multilayered laminated composite plates with arbitrarily located multiple delaminations, and presented a failure analysis of multiple delaminated plates subjected to transverse static load and impact, and a dynamic analysis of multiple delaminated composite shells. Kim et al. [19] proposed a procedure for investigation into the effects of delamination location and number of delaminations on dynamic response of composite laminates. Lee et al. [20,21] carried out free vibration analysis of through-the-width multidelaminated composite beams using the classical laminated beam theory. It was reported that the size, location, and number of multidelaminations have significant effects on the natural frequency and elastic buckling load. Cho et al. [22,23] developed a higher-order Zig-Zag theory for studying the dynamic behavior of a laminated composite structure with multiple delaminations. Wang and Yuan [24] employed a prestack reverse-time migration technique to locate multiple delaminations in a laminated plate. However, research on multiple delamination identification using smart materials is very limited. Hence, this paper will focus on modeling development for identification of multiple delaminations in laminated beams using smart material actuators and sensors.

It was noted from literature that most sensors being considered for delamination detection are passive, such as fiber optics. They can only be used for inferring the integrity and safety of a laminated composite structure under an external loading. The reliability and confidence of a delamination detection technique would be significantly improved if active, instead of passive, sensors are used because they can be used to generate preselected diagnostic signals and transmit them to neighboring sensors whose responses can then be measured and interpreted in terms of delamination location and size within a laminated structure. Magnetostrictive material is an active material having a magnetostrictive effect (i.e., when magnetostrictive material is placed in a magnetic field, they are mechanically deformed, and vice versa [25]). The recent development of giant magnetostrictive materials, e.g., Terfenol-D, has enabled for the first time the production of strains and forces sufficiently large to facilitate the use of this material in the area of actuators and sensors. Recently, magnetostrictive sensors/actuators were proposed to be used in damage detection of composite structures. An exploratory investigation was conducted by Krishnamurthy et al. [26] for studying the feasibility of detecting delaminations in polymeric laminates using magnetostrictive particle layers. However, there has been minimal research in the field of modeling development for multiple delamination detection using magnetostrictive materials.

In this paper, a dynamic analytical model is developed for identifying multiple delaminations embedded in a laminated beam, which is surface-bonded with an integrated magnetostrictive layer. The model that includes parameters characterizing multiple through-the-width delaminations is developed using the classical beam theory and the assumption of constant peel and shear strains through the bond line thickness [27]. For simplicity, the delamination front lines are assumed to be straight and perpendicular to the longitudinal direction of a beam. The contact and friction between the upper and

Presented as Paper 2177 at the 47th AIAA/ASME/ASCE/AHS/ASC Structures, Structural Dynamics & Materials Conference, Newport, Rhode Island, USA, 1–4 May 2006; received 8 February 2006; revision received 21 March 2006; accepted for publication 22 March 2006.

*Postdoctoral Fellow, School of Aerospace, Mechanical and Mechatronic Engineering, Building J11, University of Sydney, Sydney, New South Wales 2006, Australia.

†Professor, School of Aerospace, Mechanical and Mechatronic Engineering, Building J11, University of Sydney, Sydney, New South Wales 2006, Australia.

lower delaminated surfaces are not considered by assuming that there is no stress transferring between them. The influence of noise on the measured magnetic flux density is ignored in this preliminary study. An actuation coil is employed to excite the beam system and a sensing coil is used to measure the required magnetic flux density. By monitoring the difference of the predicted magnetic flux densities passing through the coils which encircles the beam with and without delaminations, the presence, location, and size of the multiple through-the-width delaminations embedded in a laminated beam can be identified. A quantitative comparison of the first three frequencies between the present analytical and finite element models is carried for verifying the present analytical model.

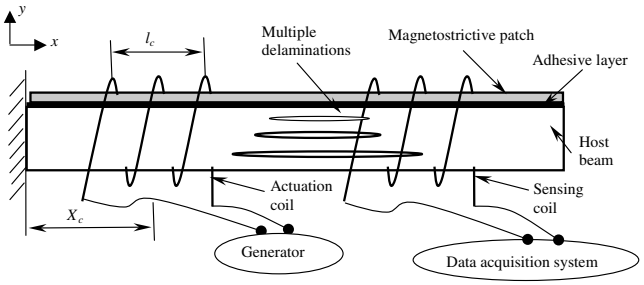

Fig. 1 Schematics of a beam system encircled by horizontal sensing and actuation coils.

II. Multiple Delamination Modeling Development

A laminated beam system with multiple through-the-width delaminations and bonded with an integrated magnetostrictive patch on its upper surface is considered and shown in Fig. 1. Since the governing equations are different for the beam segments with and without delamination, and for the magnetostrictive patch segments used as actuator or sensor, the multiple-shooting method [28] is employed to solve this problem. The beam system is first subdivided into a number of spanwise regions and the simple shooting method is used to obtain solutions by adjusting the initial values of each region. By combining the solutions for each region, a set of linear algebraic equations can be obtained and numerically solved by imposing the corresponding boundary condition at both fixed and free ends as well as the continuity conditions at the interface between two adjacent regions.

For the original-pattern case shown in Fig. 1, the beam system is divided into nine regions (see Fig. 2) and each region is composed of the magnetostrictive patch, host beam, or delaminated beam segments. Because only the delamination opening mode is considered, the stress transferring between any two adjacent delaminated beam components is ignored. Using the classical beam theory and the assumptions mentioned in the preceding section, the required dynamic equations of motion for each component can be derived. For example, the dynamic equations of motion for the components located in region 6 shown in Fig. 2 are given by

$$\rho A\ddot{u} = \partial T/\partial x + \tau b \tag{1}$$

$$\rho A\ddot{w} = \partial Q/\partial x + \sigma b \tag{2}$$

$$\partial M/\partial x - Q + \tau bt/2 = 0 \tag{3}$$

where ρ, A, b, t, u, w, T, Q, M, σ, and τ stand for density, cross-sectional area, width, thickness, longitudinal displacement, transverse displacement, longitudinal force, shear force, bending moment, and peel and shear stresses in the adhesive layer between the magnetostrictive patch and the top (or first) delaminated beam component. The values of T, M, σ, and τ can be evaluated by Eqs. (8–11) in [13]. The corresponding symbols and values for each component can be obtained from Table 1.

By taking the Fourier transformation with respect to time for all dynamic equations of motion required for the beam system, we have the following differential equations

$$\mathrm{d}\,\bar{U}_k/\mathrm{d}x = A_k\bar{U}_k \tag{4}$$

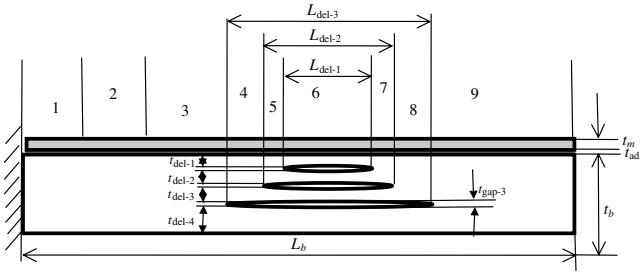

Fig. 2 Schematics of a beam system bonded with an integrated magnetostrictive patch (for the case of original-pattern).

Where over-bar represents the Fourier transformation with respect to time, $\bar{U}_k$ is the state vector and A_k is a matrix for the region k ($k = 1$–9 stand for the regions 1–9).

For the case of region 6, its corresponding state vector and matrix are given by

$$\overline{U}_6 = [\overline{U}_{6m} \quad \overline{U}_{6\text{del}-1} \quad \overline{U}_{6\text{del}-2} \quad \overline{U}_{6\text{del}-3} \quad \overline{U}_{6\text{del}-4}]^T \tag{5}$$

where $\overline{U}_{6l} = [\overline{u}_{6l} \quad \overline{w}_{6l} \quad \partial\overline{w}_{6l}/\partial x \quad \overline{T}_{6l} \quad \overline{Q}_{6l} \quad \overline{M}_{6l}]$, $l = m$, $\mathrm{del}-1$, $\mathrm{del}-2$, $\mathrm{del}-3$, and $\mathrm{del}-4$, respectively.

$$A_6 = \begin{bmatrix} A_6^{11} & A_6^{12} & 0 & 0 & 0 \\ A_6^{21} & A_6^{22} & 0 & 0 & 0 \\ 0 & 0 & A_6^{33} & 0 & 0 \\ 0 & 0 & 0 & A_6^{44} & 0 \\ 0 & 0 & 0 & 0 & A_6^{55} \end{bmatrix}$$

The matrices $A_6^{11}, A_6^{12}, A_6^{21}, A_6^{22}, A_6^{33}, A_6^{44}$ and A_6^{55} can be found in the Appendix. By solving Eq. (4), we have

$$\overline{U}_k(x_k) = C_k e^{A_k x_k} \tag{6}$$

in which $k = 1$–9 for the regions 1–9, and $x_k = 0$–l_k (l_k is the length of region k), $C_k = \overline{U}_k(x_k)|_{x_k=0}$. For the beam system shown in Fig. 1, the boundary condition after the Fourier transformation can be expressed as

$$[B_{10}]\begin{bmatrix}\overline{U}_{1m}\\ \overline{U}_{1b}\end{bmatrix}_{x=0} + [B_{9L_b}]\begin{bmatrix}\overline{U}_{9m}\\ \overline{U}_{9b}\end{bmatrix}_{x=L_b} = 0 \tag{7}$$

The matrices $[B_{10}]$ and $[B_{9L_b}]$ are given in the Appendix.

Table 1 The corresponding symbols and values for the components in region 4

Component	ρ, A, t	u, w, T, Q, M	σ, τ
Magnetostrictive patch	ρ_m, A_m, t_m	$u_{6m}, w_{6m}, T_{6m}, Q_{6m}, M_{6m}$	σ_{6m}, τ_{6m}
First delaminated beam component	$\rho_b, A_{\text{del}-1}, t_{\text{del}-1}$	$u_{6\text{del}-1}, w_{6\text{del}-1}, T_{6\text{del}-1}, Q_{6\text{del}-1}, M_{6\text{del}-1}$	$-\sigma_{6m}, -\tau_{6m}$
Second delaminated beam component	$\rho_b, A_{\text{del}-2}, t_{\text{del}-2}$	$u_{6\text{del}-2}, w_{6\text{del}-2}, T_{6\text{del}-2}, Q_{6\text{del}-2}, M_{6\text{del}-2}$	0, 0
Third delaminated beam component	$\rho_b, A_{\text{del}-3}, t_{\text{del}-3}$	$u_{6\text{del}-3}, w_{6\text{del}-3}, T_{6\text{del}-3}, Q_{6\text{del}-3}, M_{6\text{del}-3}$	0, 0
Fourth delaminated beam component	$\rho_b, A_{\text{del}-4}, t_{\text{del}-4}$	$u_{6\text{del}-4}, w_{6\text{del}-4}, T_{6\text{del}-4}, Q_{6\text{del}-4}, M_{6\text{del}-4}$	0, 0

At the interface between two consecutive regions, the continuity conditions of all displacements and the equilibrium conditions of the stress resultants must be imposed, followed by taking the Fourier transformation with respect to time.

By numerically solving differential Eq. (6) together with its corresponding boundary conditions and continuity conditions, we can obtain the natural frequency of the beam system and the average strain in each region, and then the magnetic flux density passing through each region for a selected natural frequency. To obtain the magnetic flux density distributions along the beam length, the regions 1–9 can be further divided into *N1* to *N9* subregions. The required magnetic flux density passing through a subregion k, $B_k(x_k, \omega)$ can be calculated by

$$B_k(x_k, \omega) = q_{j1m}|\epsilon_m(x_k, \omega)| \tag{8}$$

where x_k is the distance of the center for the subregion k from the fixed end, q_{j1m} is the piezomagnetic constant for the magnetostrictive patch subjected to an electric field in the j direction, $\epsilon_m(x_k, \omega)$ is the average strain measured from the magnetostrictive patch segment bonded on the beam subregion k, and ω stands for a selected natural frequency.

III. Numerical Results and Verification

To identify multiple delaminations embedded in a cantilever laminated composite beam, a baseline case with the beam length of

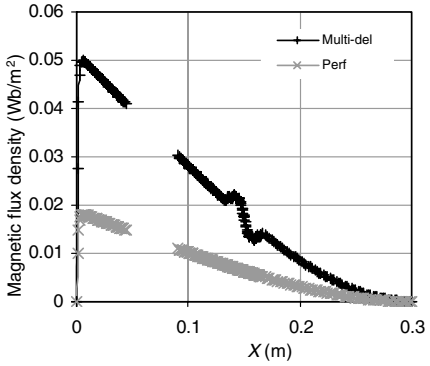

a) Variation of the magnetic flux density vs x

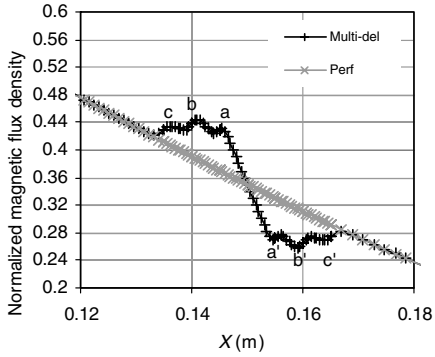

b) Variation of the normalized magnetic flux density vs x for the range of x = 0.12 m to x = 0.18 m

Fig. 3 Variation trends of the magnetic flux density and its normalized quantity vs x for the beams with and without multiple delaminations (for the case of vibration mode 1).

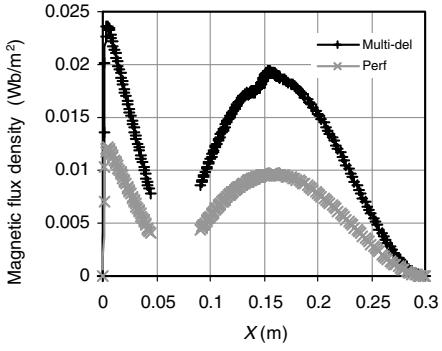

a) Variation of the magnetic flux density vs x

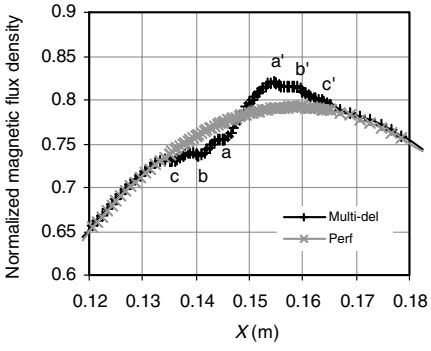

b) Variation of the normalized magnetic flux density vs x for the range of x = 0.12 m to x = 0.18 m

Fig. 4 Variation trends of the magnetic flux density and its normalized quantity vs x for the beams with and without multiple delaminations (for the case of vibration mode 2).

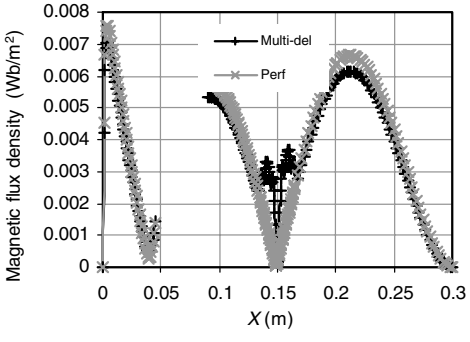

a) Variation of the magnetic flux density vs x

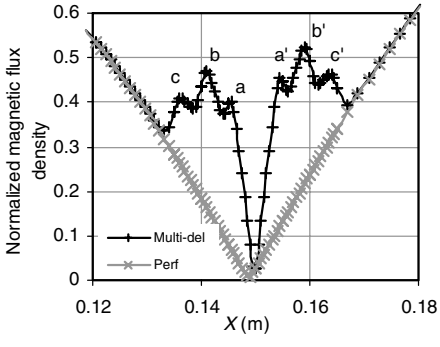

b)Variation of the normalized magnetic flux density vs x for the range of x = 0.12 m to x = 0.18 m

Fig. 5 Variation trends of the magnetic flux density and its normalized quantity vs x for the beams with and without multiple delaminations (for the case of vibration mode 3).

0.3 m, width of 0.02 m, and thickness of 1.9 mm is considered. The thickness of the magnetostrictive patch and adhesive layer are chosen to be 0.4 and 0.15 mm, respectively. The composite beam and magnetostrictive patch are made of T300/GY260 plain weave composite and Terfenol-D material. The complex Young's modulus for the host beam, Terfenol-D patch, and adhesive layer are chosen to be $65.68(1 + 0.011i)$ GPa, $22.35(1 + 0.011i)$ GPa, and $2.15(1 + 0.011i)$ GPa, respectively. The piezomagnetic constant for the Terfenol-D layer q_{11m} is selected to be 200 Wb/m^2. The density for the host beam, Terfenol-D patch, and adhesive layer are chosen as 1527.38 kg/m^3, 9250 kg/m^3, and 1600 kg/m^3, respectively [29–31]. The magnetostrictive segment bonded on region 2 functions as an actuator for exciting the beam system and the rest of the magnetostrictive segments are employed as sensors for recording the required magnetic flux density. The magnetic field applied along the magnetostrictive layer (i.e., in the x direction) in region 2 is selected to be 1000 A/m. The values of delamination length $L_{\text{del}-1}$, $L_{\text{del}-2}$, and $L_{\text{del}-3}$ are 0.01, 0.02, and 0.03 m, and those of delaminated beam component thickness $t_{\text{del}-1}$, $t_{\text{del}-2}$, $t_{\text{del}-3}$, and $t_{\text{del}-4}$ are selected to be 0.475 mm. The values of delamination gap $t_{\text{gap}-1}$, $t_{\text{gap}-2}$, and $t_{\text{gap}-3}$ (see $t_{\text{gap}-3}$ in Fig. 2) are chosen to be zero.

For the beams with and without multiple delaminations, the variation trends of the magnetic flux density and its normalized quantity vs x for the baseline and original-pattern case are obtained using the present analytical model, and are shown in Figs. 3–5 for the cases of vibration mode 1, 2, and 3, respectively. In Figs. 3–5, the blank parts in the curves indicate the size and location of the magnetostrictive segment used as actuators. The abrupt axial discontinuities in the magnetic flux density or its normalized distributions, which are measured from the magnetostrictive segments employed as sensors, clearly indicate the tips for multiple delaminations embedded in the beam system. For example, the distances between point a and a', b and b', and c and c' in Figs. 3b, 4b, and 5b are consistent with the delamination length $L_{\text{del}-1}$, $L_{\text{del}-2}$, and $L_{\text{del}-3}$, respectively. This has proven that the present model can be used to identify the presence of multiple delaminations in a beam system and to evaluate their locations and sizes.

For the purpose of verifying the present analytical model, a two-dimensional plane strain finite element analysis (FEA) model for a cantilever laminated composite beam bonded with magnetostrictive patch are developed using the FEA software Strand7 [32]. A comparison of the first three frequencies between the present analytical and FEA models for the baseline case is conducted. It is observed that the first three natural frequencies predicted using the present analytical model are in good agreement with those predicted using the FEA model. The difference between these two models is 2.1% for mode 1, 2.1% for mode 2, and 1.5% for mode 3.

IV. Conclusions

A multiple through-the-width delamination detection modeling approach has been developed for cantilever laminated beams surface-bonded with a smart magnetostrictive patch. The model was established using the classical beam theory, and under the assumptions of constant peel and shear strains through the bond line thickness, as well the assumption that there was not contact and friction between the delaminated surfaces. A magnetostrictive patch was employed as actuator for exciting the beam system and as sensor for measuring the required magnetic flux density. By monitoring the variation trend of the magnetic flux density distribution along the beam length, the presence, size, and location for the case of original-pattern can be clearly identified. A comparison of the first three natural frequencies predicted using the present analytical model with those obtained using the FEA model has revealed that there is a good agreement between these two models. This has proven that the present analytical model can be used for identifying multiple through-the-width delaminations.

Appendix: Matrices for Eqs. (4) and (6)

$$A_6^{11} = \begin{bmatrix} 0 & 0 & 0 & \frac{1}{bY_m t_m} & 0 & 0 \\ 0 & 0 & 1 & 0 & 0 & 0 \\ 0 & 0 & 0 & 0 & 0 & -\frac{12}{bY_m t_m^3} \\ \frac{bG_{\text{ad}}}{t_{\text{ad}}} - \rho_m A_m \omega^2 & 0 & -\frac{bG_{\text{ad}} t_m}{2t_{\text{ad}}} & 0 & 0 & 0 \\ 0 & \frac{bY_{\text{ad}}}{t_{\text{ad}}} - \rho_m A_m \omega^2 & 0 & 0 & 0 & 0 \\ \frac{bG_{\text{ad}} t_m}{2t_{\text{ad}}} & 0 & -\frac{bG_{\text{ad}} t_m^2}{4t_{\text{ad}}} & 0 & 1 & 0 \end{bmatrix} \quad A_6^{12} = \begin{bmatrix} 0 & 0 & 0 & 0 & 0 & 0 \\ 0 & 0 & 0 & 0 & 0 & 0 \\ 0 & 0 & 0 & 0 & 0 & 0 \\ -\frac{bG_{\text{ad}}}{t_{\text{ad}}} & 0 & -\frac{bG_{\text{ad}} t_{\text{del}-1}}{2t_{\text{ad}}} & 0 & 0 & 0 \\ 0 & -\frac{bY_{\text{ad}}}{t_{\text{ad}}} & 0 & 0 & 0 & 0 \\ -\frac{bG_{\text{ad}} t_m}{2t_{\text{ad}}} & 0 & -\frac{bG_{\text{ad}} t_m t_{\text{del}-1}}{4t_{\text{ad}}} & 0 & 0 & 0 \end{bmatrix}$$

$$A_6^{21} = \begin{bmatrix} 0 & 0 & 0 & 0 & 0 & 0 \\ 0 & 0 & 0 & 0 & 0 & 0 \\ 0 & 0 & 0 & 0 & 0 & 0 \\ -\frac{bG_{\text{ad}}}{t_{\text{ad}}} & 0 & \frac{bG_{\text{ad}} t_m}{2t_{\text{ad}}} & 0 & 0 & 0 \\ 0 & -\frac{bY_{\text{ad}}}{t_{\text{ad}}} & 0 & 0 & 0 & 0 \\ \frac{bG_{\text{ad}} t_{\text{del}-1}}{2t_{\text{ad}}} & 0 & -\frac{bG_{\text{ad}} t_m t_{\text{del}-1}}{4t_{\text{ad}}} & 0 & 0 & 0 \end{bmatrix}$$

$$A_6^{22} = \begin{bmatrix} 0 & 0 & 0 & \frac{1}{bY_b t_{\text{del}-1}} & 0 & 0 \\ 0 & 0 & 1 & 0 & 0 & 0 \\ 0 & 0 & 0 & 0 & 0 & -\frac{12}{bY_b t_{\text{del}-1}^3} \\ \frac{bG_{\text{ad}}}{t_{\text{ad}}} - \rho_b A_{\text{del}-1} \omega^2 & 0 & \frac{bG_{\text{ad}} t_{\text{del}-1}}{2t_{\text{ad}}} & 0 & 0 & 0 \\ 0 & \frac{bY_{\text{ad}}}{t_{\text{ad}}} - \rho_b A_{\text{del}-1} \omega^2 & 0 & 0 & 0 & 0 \\ -\frac{bG_{\text{ad}} t_{\text{del}-1}}{2t_{\text{ad}}} & 0 & -\frac{bG_{\text{ad}} t_{\text{del}-1}^2}{4t_{\text{ad}}} & 0 & 1 & 0 \end{bmatrix}$$

$$A_6^{kk} = \begin{bmatrix} 0 & 0 & 0 & \frac{1}{bY_b t_{\text{del}-(k-1)}} & 0 & 0 \\ 0 & 0 & 1 & 0 & 0 & 0 \\ 0 & 0 & 0 & 0 & 0 & -\frac{12}{bY_b t_{\text{del}-(k-1)}^3} \\ -\rho_b A_{\text{del}-(k-1)} \omega^2 & 0 & 0 & 0 & 0 & 0 \\ 0 & -\rho_b A_{\text{del}-(k-1)} \omega^2 & 0 & 0 & 0 & 0 \\ 0 & 0 & 0 & 0 & 1 & 0 \end{bmatrix}, \quad \text{where } k = 3, 4, 5$$

$$B_{10} = \begin{bmatrix} 0 & 0 & 0 & 1 & 0 & 0 \\ 0 & 0 & 0 & 0 & 1 & 0 \\ 0 & 0 & 0 & 0 & 0 & 1 \\ 0 & 0 & 0 & 0 & 0 & 0 \\ 0 & 0 & 0 & 0 & 0 & 0 \\ 0 & 0 & 0 & 0 & 0 & 0 \\ 1 & 0 & 0 & 0 & 0 & 0 \\ 0 & 1 & 0 & 0 & 0 & 0 \\ 0 & 0 & 1 & 0 & 0 & 0 \\ 0 & 0 & 0 & 0 & 0 & 0 \\ 0 & 0 & 0 & 0 & 0 & 0 \\ 0 & 0 & 0 & 0 & 0 & 0 \end{bmatrix},$$

$$B_{9L_b} = \begin{bmatrix} 0 & 0 & 0 & 0 & 0 & 0 \\ 0 & 0 & 0 & 0 & 0 & 0 \\ 0 & 0 & 0 & 0 & 0 & 0 \\ 0 & 0 & 0 & 1 & 0 & 0 \\ 0 & 0 & 0 & 0 & 1 & 0 \\ 0 & 0 & 0 & 0 & 0 & 1 \\ 0 & 0 & 0 & 0 & 0 & 0 \\ 0 & 0 & 0 & 0 & 0 & 0 \\ 0 & 0 & 0 & 0 & 0 & 0 \\ 0 & 0 & 0 & 1 & 0 & 0 \\ 0 & 0 & 0 & 0 & 1 & 0 \\ 0 & 0 & 0 & 0 & 0 & 1 \end{bmatrix}$$

Acknowledgments

The authors are grateful for the support of University of Sydney via University Postdoctoral Research Fellowship, and Research and Development Grant.

References

[1] Ip, K. H., and Mai, Y. W., "Delamination Detection in Smart Composite Beams Using Lamb Waves," *Smart Materials & Structures*, Vol. 13, No. 3, 2004, pp. 544–551.

[2] Toyama, N., Noda, J., and Okabe, T., "Quantitative Damage Detection in Cross-Ply Laminates Using Lamb Wave Method," *Composites Science and Technology*, Vol. 63, No. 10, 2003, pp. 1473–1479.

[3] Kessler, S. S., Spearing, S. M., and Soutis, C., "Damage Detection in Composite Materials Using Lamb Wave Methods," *Smart Materials & Structures*, Vol. 11, No. 2, 2002, pp. 269–278.

[4] Valdes, S. H. D., and Soutis, C., "Delamination Detection in Composite Laminates from Variations of Their Modal Characteristics," *Journal of Sound and Vibration*, Vol. 228, No. 1, 1999, pp. 1–9.

[5] Saravanos, D. A., and Hopkins, D. A., "Effects of Delaminations on the Damped Dynamic Characteristics of Composite Laminates: Analysis and Experiments," *Journal of Sound and Vibration*, Vol. 192, No. 5, 1996, pp. 977–993.

[6] Valdes, S. H. D., and Soutis, C., "Delamination Detection in Composite Laminates from Variations of Their Modal Characteristics," *Journal of Low Frequency Noise Vibration and Active Control*, Vol. 19, No. 1, 2000, pp. 27–33.

[7] Ueda, M., Todoroki, A., Shimamura, Y., and Kobayashi, H., "Monitoring Delamination of Laminated CFRP Using the Electric Potential Change Method: Application of Normalization Method and the Effect of the Shape of a Delamination Crack," *Advanced Composite Materials*, Vol. 13, No. 3–4, 2004, pp. 311–324.

[8] Iwasaki, A., and Todoroki, A., "Statistical Evaluation of Modified Electrical Resistance Change Method for Delamination Monitoring of CFRP Plate," *Structural Health Monitoring—An International Journal*, Vol. 4, No. 2, 2005, pp. 119–136.

[9] Todoroki, A., Tanaka, M., and Shimamura, Y., "High Performance Estimations of Delamination of Graphite/Epoxy Laminates with Electric Resistance Change Method," *Composites Science and Technology*, Vol. 63, No. 13, 2003, pp. 1911–1920.

[10] Todoroki, A., Tanaka, M., and Shimamura, Y., "Measurement of Orthotropic Electric Conductance of CFRP Laminates and Analysis of the Effect on Delamination Monitoring with an Electric Resistance Change Method," *Composites Science and Technology*, Vol. 62, No. 5, 2002, pp. 619–628.

[11] Ling, H. Y., Lau, K. T., Cheng, L., and Jin, W., "Fiber Optic Sensors for Delamination Identification in Composite Beams Using a Genetic Algorithm," *Smart Materials & Structures*, Vol. 14, No. 1, 2005, pp. 287–295.

[12] Zhou, G., and Sim, L. M., "Damage Detection and Assessment in Fiber-Reinforced Composite Structures with Embedded Fiber Optic Sensors —Review," *Smart Materials & Structures*, Vol. 11, No. 6, 2003, pp. 925–939.

[13] Tan, P., and Tong, L. Y., "Delamination Detection of Composite Beams Using Piezoelectric Sensors with Evenly Distributed Electrode Strips," *Journal of Composite Materials*, Vol. 38, No. 4, 2004, pp. 321–352.

[14] Tan, P., and Tong, L., "A Delamination Detection Model for Composite Beams Using PFRC Sensor/Actuator," *Composites, Part A: Applied Science and Manufacturing*, Vol. 35, No. 2, 2004, pp. 231–247.

[15] Tan, P., and Tong, L. Y., "Identification of Delamination in a Composite Beam Using Integrated Piezoelectric Sensor/Actuator Layer," *Composite Structures*, Vol. 66, Nos. 1–4, 2004, pp. 391–398.

[16] Parhi, P. K., Bhattacharyya, S. K., and Sinha, P. K., "Finite Element Dynamic Analysis of Laminated Composite Plates with Multiple Delaminations," *Journal of Reinforced Plastics and Composites*, Vol. 19, No. 11, 2000, pp. 863–882.

[17] Parhi, P. K., Bhattacharyya, S. K., and Sinha, P. K., "Failure Analysis of Multiple Delaminated Composite Plates due to Bending and Impact," *Bulletin of Materials Science*, Vol. 24, No. 2, 2001, pp. 143–149.

[18] Parhi, P. K., Bhattacharyya, S. K., and Sinha, P. K., "Dynamic Behavior and Impact Induced First Ply Failure of Multiple Delaminated Composite Shells," *Journal of Reinforced Plastics and Composites*, Vol. 20, No. 15, 2001, pp. 1276–1300.

[19] Kim, H. S., Chattopadhyay, A., and Ghoshal, A., "Dynamic Analysis of Composite Laminates with Multiple Delamination Using Improved Layerwise Theory," *AIAA Journal*, Vol. 41, No. 9, 2003, pp. 1771–1779.

[20] Lee, S., Park, T., and Voyiadjis, G. Z., "Free Vibration Analysis of Axially Compressed Laminated Composite Beam-Columns with Multiple Delaminations," *Composites Part B: Engineering*, Vol. 33, No. 8, 2002, pp. 605–617.

[21] Lee, S., Park, T., and Voyiadjis, G. Z., "Vibration Analysis of Multi-Delaminated Beams," *Composites Part B: Engineering*, Vol. 34, No. 7, 2003, pp. 647–659.

[22] Cho, M., and Kim, J. S., "Higher-order Zig-Zag Theory for Laminated Composites with Multiple Delaminations," *Journal of Applied Mechanics*, Vol. 68, No. 6, 2001, pp. 869–877.

[23] Oh, J., Cho, M., and Kim, J. S., "Dynamic Analysis of Composite Plate with Multiple Delaminations Based on Higher-Order Zigzag Theory," *International Journal of Solids and Structures*, Vol. 42, No. 23, 2005, pp. 6122–6140.

[24] Wang, L., and Yuan, F. G., "Damage Identification in a Composite Plate Using Prestack Reverse-Time Migration Technique," *Structural Health Monitoring—An International Journal*, Vol. 4, No. 3, 2005, pp. 195–211.

[25] Kwun, H., and Bartels, K. A., "Magnetostrictive Sensor Technology and Its Applications," *Ultrasonics*, Vol. 36, Nos. 1–5, 1998, pp. 171–178.

[26] Krishnamurthy, A. V., Anjanappa, M., Wang, Z., and Chen, X., "Sensing of Delamination in Composite Laminates Using Embedded Magnetostrictive Particle Layers," *Journal of Intelligent Material Systems and Structures*, Vol. 10, No. 10, 1999, pp. 825–835.

[27] Tong, L., and Steven, G. P., *Analysis and Design of Structural Bonded Joints*, Kluwer, Dordrecht, the Netherlands, 1999.

[28] Stoer, J., and Bulirsch, R., *Introduction to Numerical Analysis*, Springer, New York, 1980, pp. 483–59.

[29] Tong, L. Y., Sun, D. C., and Atluri, S. N., "Sensing and Actuating Behaviors of Piezoelectric Layers with Debonding in Smart Beams," *Smart Materials and Structures*, Vol. 10, No. 4, 2001, pp. 713–723.

[30] Tan, P., Tong, L., and Steven, G. P., "A Flexible 3D FEA Modeling Approach for Predicting the Mechanical Properties of Plain Weave Unit Cell," *Proceedings of the Eleventh International Conference on Composite Materials (ICCM11)*, Woodhead Publishing, Ltd., Gold Coast, Australia, Vol. 5, 14–18 July 1997, pp. 67–76.

[31] Claeyssen, F., Lhermet, N., and Grosso, G., "Giant Magnetostrictive Alloy Actuators," *International Journal of Applied Electromagnetics in Materials*, Vol. 5, 1994, pp. 67–73.

[32] Introduction to the Strand7 Finite Element Analysis System, G+D Computing Pty., Ltd., Sydney, Australia, 1999.

A. Palazotto
Associate Editor